Compositional Mismatch between Chemical Patterns on a Substrate and Polymer Blends Yielding Spin-Cast Films with Subpattern Periodicity

J. Raczkowska,[†] A. Bernasik,[‡] A. Budkowski,*[,†] J. Rysz,[†] B. Gao,[§] and M. Lieberman[§]

M. Smoluchowski Institute of Physics, Jagellonian University, Reymonta 4, 30-059 Kraków, Poland; Faculty of Physics and Nuclear Techniques, AGH - University of Science and Technology, Mickiewicza 39, 30-059 Kraków, Poland; Department of Chemistry and Biochemistry, University of Notre Dame, Notre Dame, Indiana 46556

Received November 14, 2006; Revised Manuscript Received January 31, 2007

ABSTRACT: Two blends (1:1 and 5:3 w:w) of poly(2-vinylpyridine) (PVP) and partly brominated polystyrene were spin-cast (with constant inherent domain scale $2R = 4.2 \pm 0.5$ μm) onto a gold substrate which had been microcontact printed with stripes of hexadecanethiol SAM. Two chemical patterns on the substrate were used, one with symmetrical stripes (4 μm Au/4 μm hexadecane SAM) and the other with narrow gold stripes and wider SAM stripes (3 μm/5 μm). The resulting film morphologies were mapped with atomic force microscopy. Secondary ion mass spectrometry shows that raised regions on the film surface correspond to PVP-rich domains, and the surface polymer composition extends all the way down to the substrate. Fourier analysis reveals structural modes (λ/n) smaller than the pattern periodicity $\lambda = 8$ μm. PVP preferentially adsorbs to the gold regions of the pattern. For the asymmetric pattern, which has a relatively small Au area interacting with the PVP, the fundamental mode ($n = 1$) is extinguished and higher-order substructures ($n > 1$) are seen. Use of a PVP-rich blend increases the intensity of the $n = 3$ mode and reduces that of the $n = 2$ mode. When both blend and pattern were asymmetric, both $\lambda/2$- and $\lambda/3$-substructures were observed, and the fundamental pattern periodicity was extinguished.

1. Introduction

Multicomponent polymer thin films with controlled morphology are technologically important in diverse fields, ranging from bioactive patterns[1] and lithographic templates[2] to polymer electronics.[3] The arrangement and size of domains which form functional elements have decisive impacts on device performance, e.g., in photovoltaics, LEDs, FETs, and electronic circuits composed of polymer blends.[3−5]

To obtain long-range order for lateral domain structures, films of copolymers or polymer blends are often exposed to surface patterns (with periodicity λ).[6−10] Surface pattern replication is controlled by many parameters, mainly by the competition between surface and interfacial energy[11−15] and by the match between λ and the polymer's inherent domain scale $2R$.[6,7,9,10,16] Even 3-dimensional structures can be created with the proper polymer material and surface pattern.[17]

For polymer blend films, the domain scale $2R$ increases in the course of phase separation,[18] which is initiated and sustained by elevated temperature[19] or presence of solvent.[20−22] Pattern-guided structure formation, reported for both temperature-quenched[8,10,23−27] and spin-cast (solvent-quenched)[4,5,7,8,9,16,27−36] polymer mixtures, is driven by selective polymer adsorption to the pattern. The best ordered lateral domains were obtained for $2R \sim \lambda$.[9,10,16,23,24,29,34,36] However, Fourier analysis has also revealed lateral domains with quantized length scales of λ/n (n is an integer)[16,23,24,29,34] with (relative) intensities I_n excited for $2R \sim \lambda/n$.[23,24,29,34] Very weak higher frequency modes ($n > 1$) were observed during blend annealing, and reflected free surface undulations coupled with phase separation.[23,24] Such higher frequency modes correspond to lateral domains that are smaller than the features of the surface pattern, thus potentially increasing the resolution of the polymer features beyond that of the lithographic template used to pattern the surface.

Spin-casting a polymer blend onto a patterned surface is a technologically attractive way to form polymer thin films. It offers a one-step procedure to simultaneously deposit and align different domains, e.g., functional LED elements.[5] However, it is difficult to control all related processes (e.g., breakup of transient multilayer structure and subsequent lateral phase coarsening),[37−42] which can lead to inhomogeneities in the polymer domains.[34]

In our previous work with spin-cast blends with $2R \sim \lambda/2$ and patterned surfaces with periodicity λ, the excited $\lambda/2$-substructures dominated over the domains periodic with λ ($I_2 > I_1$):[29,34] The contribution I_2 of $\lambda/2$-substructures was maximal when interfacial tension was reduced by addition of a compatibilizer to the polymer blend.[29,34] It also depended on the match between the area of the adherent region of the symmetric surface pattern and the blend fraction of selectively attracted polymer.[34,36]

In this paper, we describe a novel effect of spin-casting polymer blends with characteristic length scale $2R = \lambda/2$ onto asymmetrical micron-scale chemical patterns with periodicity λ. We find that the intensity of the fundamental structural mode was reduced to zero and higher frequency modes were enhanced when a surface template of evenly spaced hydrophobic and hydrophilic stripes was exchanged for an asymmetric surface template. This resembles graphoepitaxy of block copolymer structures, although at the larger domain sizes characteristic of polymer blends.[43,44] Using this method, domain structures with periodicity of $\lambda/2$ and $\lambda/3$ can be produced from a template with a periodicity of λ.

2. Experimental Section

Preparation of Polymer Films. Polymers used in this study were poly(2-vinylpyridine) (PVP, molecular weight $M_w = 115$K, poly-

* Corresponding author. E-mail: ufbudkow@cyf-kr.edu.pl.
† Jagellonian University of Kraków.
‡ AGH - University of Science and Technology, Kraków.
§ University of Notre Dame.

10.1021/ma062614f CCC: $37.00
Published on Web 02/27/2007

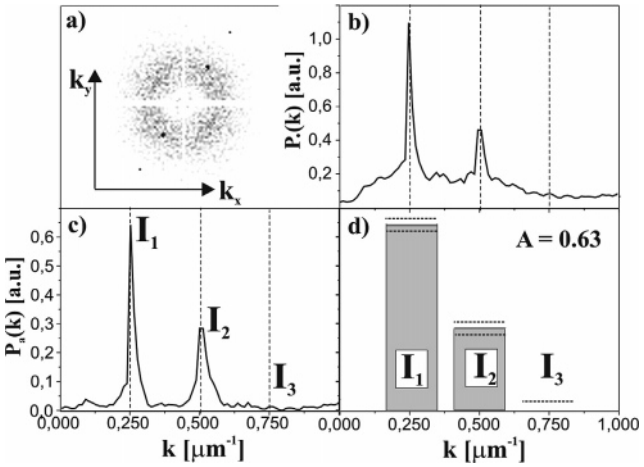

Figure 1. Fast Fourier transform analysis of AFM image shown in Figure 2a: (a) FFT transform; (b) its total power spectrum $P(k)$; (c) the spectrum $P_a(k)$ of anisotropic component as obtained from $P(k)$; (d) corresponding histogram. I_n denotes relative intensity of peaks positioned at $n\boldsymbol{k}_\lambda$ ($|\boldsymbol{k}_\lambda| = 1/\lambda$), and A reflects $P_a(k)$ contribution to $P(k)$ (see text).

dispersity index $M_w/M_n = 1.02$) and partly brominated polystyrene (PBrS, $M_w = 185$K, $M_w/M_n = 1.04$, with $x = 10.7\%$ segments brominated), purchased from Polymer Standards Service, Mainz and used as obtained to prepare binary blends 1:1 and 5:3 (mass fractions of PVP:PBrS). All blends were spin-cast (with KW-4A apparatus, Chemat Technology) in the same conditions (coating speed $\omega = 5800$ rpm, total polymer concentration $c_p = 10.7$ mg/mL) from tetrahydrofuran (THF) solution into 60 ± 7 nm thick films (as determined with atomic force microscope AFM).[22] The films were cast on homogeneous (SAM) or patterned (Au/SAM) substrates, formed by self-assembled monolayers (SAMs) of hexadecanethiol [$HS(CH_2)_{15}CH_3$] deposited or microcontact printed,[45] respectively, on Au-covered Si wafers (see previous works[16,22,29,34,36,37] for details). The dimensions of the Au/SAM stripe patterns were 4 μm/4 μm and 3 μm/5 μm (a 2 μm/2 μm pattern was used to compare the data with ref 34).

Surface and Film Characterization. The topographies of films formed on homogeneous and patterned substrates were recorded by AFM (CP Park Scientific Instruments, contact mode, Si_3N_4 tip, typical load of 4 nN). Each film on the substrate pattern was also examined with the composition mapping mode of dynamic secondary ion mass spectrometry dSIMS (VSW apparatus with high-resolution ion gun, double lens, liquid metal source, produced by Fei Co.), yielding PVP distribution maps (CN^- ions, $m/z = 26$), recorded for subsequent depths, typically with submicron lateral resolution.[46] The PVP distribution maps at various depths match the raised areas observed in the AFM images, so surface topography is a good indicator of polymer composition throughout the polymer film.

3. Results and Discussion

3.1. Fourier Analysis. Film morphologies were examined with Fourier analysis.[16,29,34] For each AFM image a 2-dimensional fast Fourier transform (FFT) was computed. FFT spectra of isotropic morphologies, such as those derived from polymer blend films on homogeneous SAMs, are characterized by an isotropic diffuse ring with $|\boldsymbol{k}| = k^*$. The radial average $P_i(k)$ of the squared FFT amplitudes was used to determine the radius k^* of the ring at its maximum. For the fixed spin-casting conditions and polymer blends used, a constant inherent domain scale $2R = 1/k^* = 4.2 \pm 0.5$ μm was obtained in this study. FFT spectra of anisotropic morphologies, such as those derived from polymer blend films on hydrophilic/hydrophobic striped surfaces, exhibit two components, shown in Figure 1. In addition to the isotropic ring, there is a slanting line of diffraction peaks

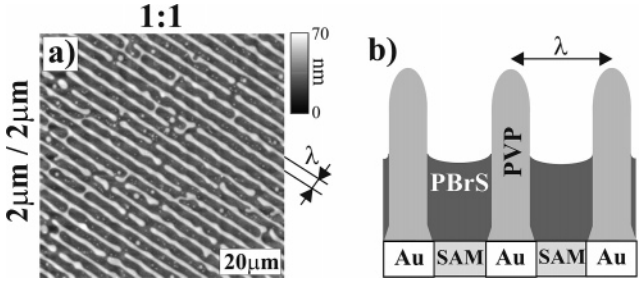

Figure 2. (a) AFM image recorded for 1:1 PVP:PBrS blend cast on 2 μm/2 μm Au/SAM pattern. Higher (light) and lower (dark) regions correspond to PVP and PBrS, respectively. (b) Sketch to illustrate sectional view of corresponding phase domain arrangement.

with $\boldsymbol{k} = n\boldsymbol{k}_\lambda$ ($|\boldsymbol{k}_\lambda| = 1/\lambda$). The squared FFT amplitudes of the $\boldsymbol{k}$-region forming a narrow stripe along the $n\boldsymbol{k}_\lambda$ peaks were averaged to yield the total power spectrum $P(k)$. The isotropic contribution $P_i(k)$, defined by the radial averaged data of the $\boldsymbol{k}$-plane without the $n\boldsymbol{k}_\lambda$ -stripe, was removed from the total spectrum $P(k)$ to yield the spectrum $P_a(k)$ of the anisotropic component. The ratio $A = \tilde{P}_a/\tilde{P}$ of the integrated power spectra $P_a(k)$ and $P(k)$, is defined as a measure of morphological anisotropy.[34] The spectrum $P_a(k)$ exhibits several peaks positioned at $n\boldsymbol{k}_\lambda$, characterized by absolute $J_n = J(n\boldsymbol{k}_\lambda)$ and relative intensities $I_n = J_n/\Sigma_m J_m$. The latter are used to measure contribution of different modes (λ/n, $n = 1, 2, 3, ...$) to the morphology of the polymer film.

3.2. Blends of PVP and PBrS on Homogeneous SAMs. To understand adsorption-driven alignment of polymer phase domains on patterned SAMs, it is necessary to study the phase separation which occurs on homogeneous hexadecanethiol SAMs. PVP:PBrS mixtures, spin-cast from THF onto homogeneous SAMs, form lateral domain structure extending from the substrate through the film to the free surface, as indicated by AFM and dSIMS results.[16] Such behavior is similar to that reported for the PVP mixture with deuterated polystyrene (PVP:dPS).[16,34,36] The PBrS polymer is very similar to plain PS,[16] and the general features of structure formation during spin-casting[38−42] can be explained on the basis of more extensive PVP:dPS data.[34] During spin-casting, phase separation, initiated by evaporating solvent, takes place simultaneously with a radial liquid flow, which controls final film thickness h. The initial multilayer phase arrangement is broken up by interfacial instability into a lateral phase structure with the scale $2R$ increased by quasi-2D coarsening. Bicontinuous (or droplet-type) morphologies were observed in 1:1 PVP:dPS, as a result of dominant (or just initiated) lateral coarsening.[34] Both phase coarsening and film thinning are terminated when polymer molecules are no longer mobile, and the scaling $h \sim 2R \sim c_p/\omega^{1/2}$ was observed.[34] PVP, which is less soluble in THF, vitrifies (due to solvent removal)[47] earlier than PBrS, leading to the collapse of initially swollen PBrS-rich areas below the level of the PVP phase. Therefore, in the final solvent-free films, PVP domains are elevated and the domain structure is correlated with film topography. AFM images recorded for PVP:PBrS films on hexadecanethiol SAMs (see Figure S1 of the Supporting Information) show bicontinuous domain structures for 1:1 blends, and similar morphology with dominant PBrS-rich droplets for 5:3 mixtures. The structure observed for 1:1 PVP:PBrS films suggests a dominant role for phase coarsening. This explains also the morphological change from 1:1 (PVP weight fraction $\Phi = 0.5$) to 5:3 mixture ($\Phi = 0.625$) further away from the critical blend composition $\Phi_C = 0.55$. In contrast, the blends spin-cast on homogeneous Au surfaces form bilayers PBrS/PVP, with the more polar PVP next

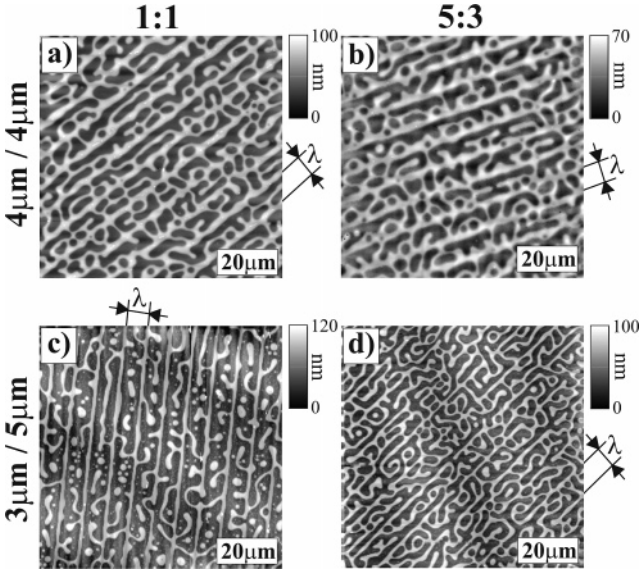

Figure 3. AFM images, recorded for PVP:PBrS blends 1:1 (a, c) and 5:3 (b, d) cast on Au/SAM patterns 4 μm/4 μm (a, b) and 3 μm/5 μm (c, d). Higher (light) and lower (dark) regions correspond to PVP and PBrS, respectively.

togold, as demonstrated earlier with different techniques (depth profiling dSIMS mode, AFM combined with selective dissolution).[16]

3.3. Blends of PVP and PBrS on Au/SAM Patterns. The organization of lateral domains of PVP:PBrS films on Au/SAM patterns is driven by the strong affinity of PVP for Au surface regions.[16] When the characteristic length scale *2R* of the polymer blend is equal to the periodicity λ of the chemical pattern, the PVP-rich phase wetting the Au stripes forms linear PVP domains with a periodicity of λ (Figure 2a). When the characteristic length scale of the polymer is smaller than the pattern periodicity, as in this work, where $2R/\lambda \sim 0.53 \pm 0.06$, the PVP domains positioned on hydrophobic SAM stripes (which attract neither PVP nor PBrS)[16] form substructures with a periodicity close to λ/n (Figure 3). The transition from the λ-structure (Figure 2a) into a morphology with $\lambda/2$-substructure (Figure 3a) was obtained by doubling the periodicity of the symmetric substrate pattern for the 1:1 PVP:PBrS blend. An analogous transition in 1:1 PVP:dPS, induced by reduction of the structural scale *2R*, was accompanied by the change from continuous PVP domains into isolated PVP domains.[34] The coexistence of continuous lateral PVP domains with visible $\lambda/2$-substructure implies extensive interfaces, possible for PVP:PBrS (or PVP:PMMA:dPS)[34] which have interfacial energy lower than that for PVP:dPS.[16] Due to the reduction of $2R/\lambda$ from $\sim$1 to $\sim$1/2, the morphological anisotropy *A* was decreased by one-third, while the intensity I_1 of the fundamental morphological mode was reduced by about 50% and that of the $\lambda/2$ mode was increased by a similar amount (compare Figures 1d and 4a).

Central results of this study are the AFM images in Figure 3. They show morphologies of symmetric (1:1) and asymmetric (5:3) PVP:PBrS blends, both with $2R = 4.2 \pm 0.5$ μm, spin-cast on symmetric (4 μm/4 μm) and asymmetric (3 μm/5 μm) surface patterns of hexadecanethiol on gold. PVP distribution maps imaged for these film blends are represented in Figure 5 (see also the Supporting Information). Almost identical PVP maps are recorded for successive depths in the studied films (Figure 5 and Figures S2−S4). The complementary PBrS maps (with much weaker Br^- signal; see Figure S4) are consistent with this observation.

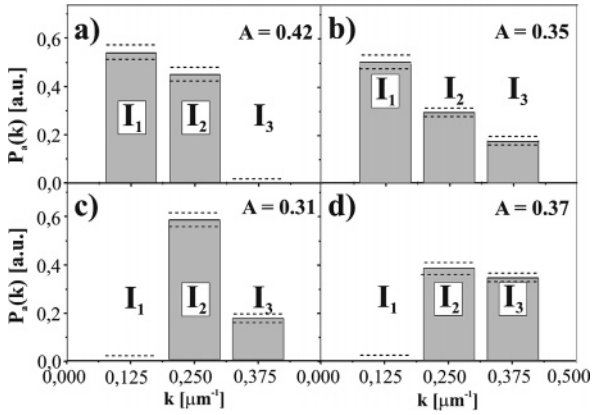

Figure 4. Histograms of relative intensities I_n and morphological anisotropy *A* values (a−d) corresponding to Figure 3, parts a−d, respectively.

The compliance of the blend film morphology with the substrate pattern depends strongly on the compositional match between the PVP blend fraction Φ and the Au pattern fraction *f*. The morphology of a symmetric blend on a symmetric pattern (1:1 on 4 μm/4 μm, $\Phi/f = 1$) shows thick PVP lines on the Au stripes, connected to elongated domains of PVP substructures on the hydrophobic SAM regions (Figures 3a and 4a). The intensities of the $\lambda/2$ and λ modes were about equal ($I_2 \sim I_1$). Compositional mismatch was introduced to this system by using either an asymmetric polymer blend (Figures 3b and 4b) or an asymmetric chemical pattern (Figures 3c and 4c). We also combined an asymmetric blend and an asymmetric pattern (Figures 3d and 4d). For the asymmetric blend (5:3 on 4 μm/4 μm, $\Phi/f = 1.25$), thick PVP-rich lines give rise to a strong periodicity of λ; on the SAM stripes we observe numerous extensions which contribute to the $\lambda/2$ and $\lambda/3$ mode. The PVP domains on the hydrophobic regions are sporadically elongated (reduced I_2) and often enclose small ($\sim\lambda/6$) PBrS droplets with a characteristic length scale of $\lambda/3$ (increased I_3). For the asymmetric pattern (1:1 on 3 μm/5 μm, $\Phi/f = 1.33$), the PVP lines on the Au stripes are as wide as the $\lambda/2$-substructures which form on the hexadecanethiol SAM. The fundamental period of $2R = \lambda$ is not observed ($I_1 = 0$); instead we see increased I_2 and I_3. When both blend and pattern are asymmetric (5:3 on 3 μm/5 μm, $\Phi/f = 1.67$) the previous effects are superimposed: PVP ribbons form elongations on Au stripes and similar extensions and loops, enclosing PBrS droplets, are formed on the SAM regions ($I_1 = 0$, I_3 increased at the expense of I_2).

Fourier analysis reveals systematic changes introduced by asymmetric blend (reduced I_2, increased I_3) (Figure 4a → 4b and Figure 4c → 4d) or asymmetric pattern ($I_1 = 0$, increased I_2 and I_3) (Figure 4a → 4c and Figure 4b → 4d), observed in each case for two modified morphologies. The effects of compositional mismatch cannot be described by a single parameter Φ/f and hardly influence the measure *A* of morphological anisotropy. The average value of *A* is 0.37 ± 0.05, higher than threshold value for discernible anisotropy $\sim$0.1.[34] This indicates that the film structure is largely induced by the substrate pattern. The relatively small ($\sim$40%) decrease in *A* for $2R/\lambda \sim 1/2$, as compared to the $2R/\lambda \sim 1$ situation (Figure 1d), resembles behavior determined previously for blends with a continuous PVP phase and low interfacial tension (PVP:PMMA:dPS).[34]

3.4. Origins of λ/n-Substructures and Subpattern Periodicity. The anisotropic morphologies of Figure 3 result from selective wetting of the Au stripes by PVP and from lateral coarsening. In this blend, lateral coarsening is driven by

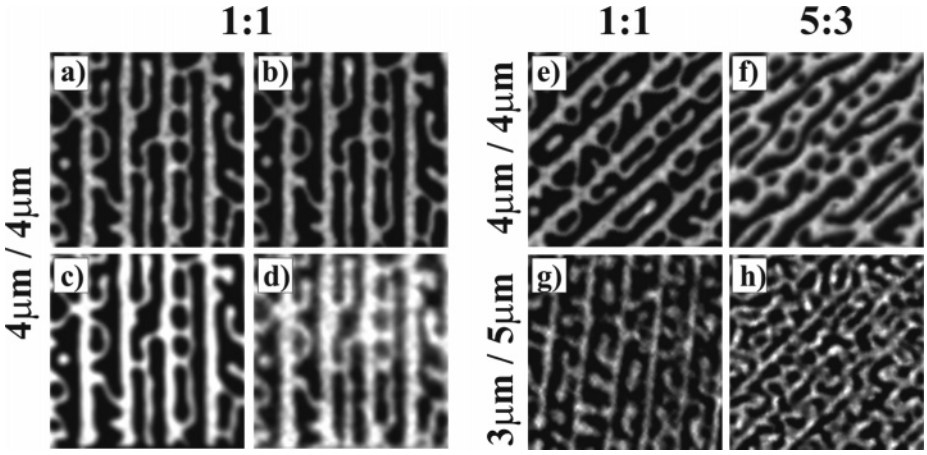

Figure 5. dSIMS maps of PVP distribution at distance $z \sim 8$ (a), 23 (b, e−h), 38 (c) and 53 nm (d) from the free surface of PVP:PBrS blends 1:1 (a−e, g) and 5:3 (f, h) cast on Au/SAM patterns 4 μm/4 μm (a−f) and 3 μm/5 μm (g, h). Light regions correspond to PVP domains.

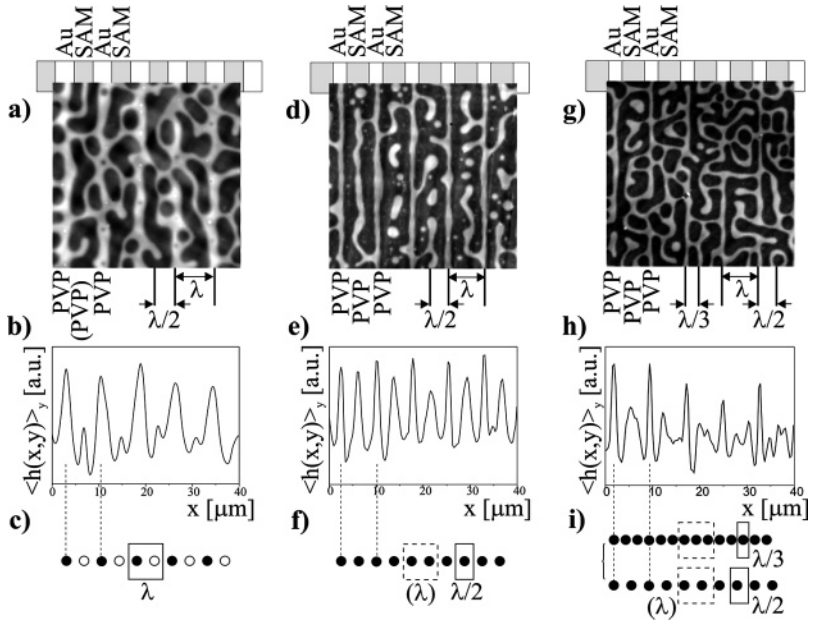

Figure 6. Selected regions of AFM images (a, d, g), their y-axis averaged height profiles $\langle h(x,y)\rangle_y$ (b, e, h) and corresponding analogies of 1-dim crystals (c, f, i) for PVP:PBrS blends 1:1 (a−f) and 5:3 (g−i) cast on Au/SAM patterns 4 μm/4 μm (a−c) and 3 μm/5 μm (d−i). AFM images (a, d, g) are positioned on the sketches of corresponding Au/SAM patterns. Higher (light) and lower (dark) regions correspond to PVP and PBrS, respectively. Different (b) and similar (e) peak areas or superimposed peaks (h) in $\langle h(x,y)\rangle_y$ correspond to model atoms in 1-dim lattices described by "unit cells" with parameter λ (c), $\lambda/2$ (f), and $\lambda/2$ and $\lambda/3$ [intergrowth structure] (i), respectively.

hydrodynamic flow through continuous PVP tubes.[34] This is why PVP domains on SAM regions are generally connected with PVP lines on Au (see Figure 6, parts a, d, g). The PVP lines on gold deplete adjacent regions of PVP, which causes the PVP areas on the hydrophobic SAM to be (locally) parallel to the Au stripes. Therefore, the spacing between PVP domains on the hexadecane SAM, in the direction normal to the Au stripes, must be a fraction λ/n of the stripe periodicity λ. While the strongest quantized (λ/n) structural modes are observed for inherent domain scales $2R \sim \lambda/n$ (with $2R$ adjusted by spin-casting),[29,34] they are also visible further away from such values. For instance, the intensity I_1 of the fundamental mode is only slightly reduced for $2R$ changed from $\sim\lambda$ to $\sim\lambda/2$ (compare Figures 1d and 4a). Even for the $\lambda/2$-substructure, the relation I_2 vs $2R/\lambda$ yields half-width at half-maximum HWHM > 0.13 (and is dependent on blend composition).[34] Also here, for $2R/\lambda = 0.53 \pm 0.06$, $\lambda/2$-modes coexist with the domains of higher ($n = 3$) or fundamental ($n = 1$) modes.

For asymmetric surface patterns, film morphologies are no longer periodic with λ (Figure 3, parts c and d). This situation is reflected by systematic absence of the peak $n = 1$ in the Fourier spectra (Figure 4). The templates induce anisotropic film morphology in the direction normal to the hydrophilic Au stripes. Long-range 1D ordering is confirmed by the line of diffraction peaks $\boldsymbol{k} = n\boldsymbol{k}_\lambda$ in the FFT and can be seen in the averaged height profiles $\langle h(x,y)\rangle_y$ (Figure 6, parts b, e, and h) plotted perpendicular to the direction of the stripes in the template.[23,24] For a 1:1 PVP:PBrS blend on the symmetric surface template, the $\langle h(x,y)\rangle_y$ profile (Figure 6, parts b and c) has constant λ and a "unit cell" with 2 different PVP-rich regions, located on the Au and the SAM stripes, respectively. The same 1:1 blend on the asymmetric pattern (Figure 6d) results in the $\langle h(x,y)\rangle_y$ profile of Figure 6e, which corresponds (by crystallographic analogy)[48] to a λ-"unit cell" with a systematically absent diffraction peak $n = 1$,[49,50] or equivalently to a new $\lambda/2$-"unit cell".

When both blend and pattern are asymmetric, we observe in the $\langle h(x,y)\rangle_y$ profile (Figure 6h) two series of individual peaks with $\lambda/2$- and $\lambda/3$- periodicity (Figure 6, parts g and i), superimposed with similar contribution. Both have high (PVP-rich) domains on Au stripes. Therefore, their areas are roughly twice as large as those of the PVP-rich domains on SAM regions. The situation in Figure 6h resembles a commensurate intergrowth structure[51] with two subsystems (Figure 6i), described by λ-"unit cells" containing 2 or 3 identical equally spaced atoms. For each subsystem the Fourier peak $n = 1$ is systematically absent.[52] Equivalently the film morphology is characterized by new $\lambda/2$ and $\lambda/3$ "unit cells" with comparable coverage.

The chemical pattern stamped onto the surface influences the position and orientation of the polymer domains. Surface relief structures are also reported to align clusters of locally ordered copolymer microdomains,[43,44] but the SAM height (<2 nm) is negligible compared with the film thickness (60 nm). Other factors such as the match between the areas of hydrophobic and hydrophilic patches and the polymer blend composition contribute to the observed domain spacings λ/n. In contrast to block copolymer films deposited on patterned substrates, where the domain size is determined by the size of the polymer blocks, here the local domain order and spacing λ/n are both imposed by the surface pattern.

4. Summary and Conclusions

To summarize, quantized morphological modes (with characteristic periods of λ/n) form in blends of PVP and PBrS that are spin-cast onto hexadecane SAM stripes on gold. Selective adsorption of PVP on the hydrophilic gold regions and interactions between the polymer phases drive domain formation. When the surface area of exposed gold in a SAM pattern is too small for the PVP volume fraction in the polymer blend, spin-cast films lack the expected periodicity λ. The fundamental mode is extinguished and substructures with λ/n ($n > 1$) are enhanced. When the PVP becomes a majority (rather than symmetric) blend component, the contribution I_3 of mode $n = 3$ is increased and that of the $\lambda/2$-substructure is reduced. Both effects combined with the adjusted inherent domain scale $2R$ allow for a pattern-guided alignment of blend structures with domains much smaller (here even $\lambda/6$) than the pattern periodicity λ. Surface stamping and spin-casting are very simple processes which could be useful for fabrication of polymer domains over large areas, and a logical direction for this work will be to see whether smaller domain sizes can be accessed through different polymer blends and surface patterns with smaller periodicity.

Acknowledgment. This work was partially supported by the Reserve of the Rector of the Jagellonian University. J. Raczkowska is grateful to the Foundation for Polish Science for financial support.

Supporting Information Available: Figures showing AFM images of PVP:PBrS film blends on a homogeneous SAM substrate (Figure S1) and dSIMS maps of composition distribution in PVP:PBrS film blends on Au/SAM patterns (Figures S2−S4). This material is available free of charge via the Internet at http://pubs.acs.org.

References and Notes

(1) Vörös, J.; Blätter, T.; Textor, M. *MRS Bull.* **2005**, *Mar*, 202. Liu, G.; Zhao, J. *Langmuir* **2006**, *22*, 2923. Yan, M.; Barlett, M. *Nano Lett.* **2002**, *2*, 275.
(2) Hamley, I. W. *Nanotechnology* **2003**, *14*, R39. Park, C.; Yoon, J.; Thomas, E. L. *Polymer* **2003**, *44*, 6725. Li, M.; Coenjarts, C. A.; Obser, C. K. *Adv. Polym. Sci.* **2005**, *190*, 183.
(3) Arias, A. C. *J. Macromol. Sci.* **2006**, *46*, 103. Moons, E. *J. Phys.: Condens. Matter* **2002**, *14*, 12235. Sirringhaus, H. *Adv. Mater.* **2005**, *17*, 2411.
(4) Coffey, D. C.; Ginger, D. S. *J. Am. Chem. Soc.* **2005**, *127*, 4565.
(5) Fichet, G.; Corcoran, N.; Ho, P. K. H.; Arias, A. C.; MacKenzie, J. D.; Huck, W. T. S.; Friend, R. H. *Adv. Mater.* **2004**, *16*, 1908.
(6) Fasolka, M. J.; Harris, D. J.; Mayes, A. M.; Yoon, M.; Mochrie, S. G. J. *Phys. Rev. Lett.* **1997**, *79*, 3018.
(7) Rockford, L.; Liu, Y.; Mansky, P.; Russell, T. P.; Yoon, M.; Mochrie, S. G. J. *Phys. Rev. Lett.* **1999**, *82*, 2602.
(8) Krausch, G.; Kramer, E. J.; Rafailovich, M. H.; Sokolov, J. *Appl. Phys. Lett.* **1994**, *64*, 2655.
(9) Böltau, M.; Walheim, S.; Mlynek, J.; Krausch, G.; Steiner, U. *Nature (London)* **1998**, *391*, 877.
(10) Karim, A.; Douglas, J. F.; Lee, B. P.; Glotzer, S. C.; Rogers, J. A.; Jackman, R. J.; Amis, E. J.; Whitesides, G. M. *Phys. Rev. E* **1998**, *57*, R6273.
(11) Wang, Q.; Nath, S. K.; Graham, M. D.; Nealey, P. F. *J. Chem. Phys.* **2000**, *112*, 9996.
(12) Kielhorn, L.; Muthukumar, M. *J. Chem. Phys.* **1999**, *111*, 2259.
(13) Shou, Z.; Chakrabarti, A. *Polymer* **2001**, *42*, 6141.
(14) Seok, C.; Freud, K. F.; Szleifer, I. *J. Chem. Phys.* **2000**, *112*, 6452.
(15) Li, X.; Denn, M. M. *Ind. Eng. Chem. Res.* **2004**, *43*, 354.
(16) Cyganik, P.; Bernasik, A.; Budkowski, A.; Bergues, B.; Kowalski, K.; Rysz, J.; Lekki, J.; Lekka, M.; Postawa, Z. *Vacuum* **2001**, *63*, 307. Budkowski, A.; Bernasik, A.; Cyganik, P.; Rysz, J.; Brenn, R. *e-Polym.* **2002**, 006.
(17) Daoulas, K. C.; Müller, M.; Stoykovich, M. P.; Park, S.-M.; Papakonstantopoulos, Y. J.; de Pablo, J. J.; Nealey, P. F.; Solak, H. H. *Phys. Rev. Lett.* **2006**, *96*, 036104.
(18) Krausch, G. *Mater. Sci. Eng.* **1995**, *R14*, 1. Binder, K. *Adv. Polym. Sci.* **1999**, *138*, 1. Budkowski, A. *Adv. Polym. Sci.* **1999**, *148*, 1. Geoghegan, M.; Krausch, G. *Prog. Polym. Sci.* **2003**, *28*, 261.
(19) Sung, L.; Karim, A.; Douglas, J. F.; Han, C. C. *Phys. Rev. Lett.* **1996**, *76*, 4368.
(20) Dalnoki-Veress, K.; Forrest, J. A.; Stevens, J. R.; Dutcher, J. R. *J. Polym. Sci., Part B: Polym. Phys.* **1996**, *34*, 3017.
(21) Walheim, S.; Böltau, M.; Mlynek, J.; Krausch, G.; Steiner, U. *Macromolecules* **1997**, *30*, 4995.
(22) Cyganik, P.; Budkowski, A.; Raczkowska, J.; Postawa, Z. *Surf. Sci.* **2002**, *507−510*, 700.
(23) Ermi, B. D.; Nisato, G.; Douglas, J. F.; Rogers, J. A.; Karim, A. *Phys. Rev. Lett.* **1998**, *81*, 3900.
(24) Nisato, G.; Ermi, B. D.; Douglas, J. F.; Karim, A. *Macromolecules* **1999**, *32*, 2356.
(25) Yoo, P. J.; Suh, K. Y.; Lee, H. H. *Macromolecules* **2002**, *35*, 3205.
(26) Li, X.; Wang, Z.; Cui, L.; Xing, R.; Han, Y.; An, L. *Surf. Sci.* **2004**, *571*, 12.
(27) Jerome, J.; Zhu, S.; Seo, Y. S.; Ho, M.; Pernodet, N.; Gambino, R.; Sokolov, J.; Rafailovich, M. H.; Zaitsev, V.; Schwarz, S.; DiNardo, R. *Macromolecules* **2004**, *37*, 6504.
(28) Fukunaga, K.; Elbs, H.; Krausch, G. *Langmuir* **2000**, *16*, 3474.
(29) Cyganik, P.; Budkowski, A.; Steiner, U.; Rysz, J.; Bernasik, A.; Walheim, S.; Postawa, Z.; Raczkowska, J. *Europhys. Lett.* **2003**, *62*, 855.
(30) Sprenger, M.; Walheim, S.; Schäffer, C.; Steiner, U. *Adv. Mater.* **2003**, *15*, 703.
(31) Walheim, S.; Schäffer, C.; Steiner, U. *Surf. Interface Anal.* **2004**, *36*, 195.
(32) Minelli, C.; Geissbuehler, I.; Eckert, R.; Vogel, H.; Heinzelmann, H.; Liley, M. *Colloid Polym. Sci.* **2004**, *282*, 1274.
(33) Li, X.; Xing, R.; Zhang, Y.; Han, Y.; An, L. *Polymer* **2004**, *45*, 1637.
(34) Raczkowska, J.; Cyganik, P.; Budkowski, A.; Bernasik, A.; Rysz, J.; Raptis, I.; Czuba, P.; Kowalski, K. *Macromolecules* **2005**, *38*, 8486.
(35) Cui, L.; Zhang, Z.; Li, X.; Han, Y. *Polym. Bull. (Berlin)* **2005**, *55*, 131.
(36) Raczkowska, J.; Bernasik, A.; Budkowski, A.; Cyganik, P.; Rysz, J.; Raptis, I.; Czuba, P. *Surf. Sci.* **2006**, *600*, 1004.
(37) Budkowski, A.; Bernasik, A.; Cyganik, P.; Raczkowska, J.; Penc, B.; Bergues, B.; Kowalski, K.; Rysz, J.; Janik. J. *Macromolecules* **2003**, *36*, 4060.
(38) Sprenger, M.; Walheim, S.; Budkowski, A.; Steiner, U. *Interface Sci.* **2003**, *11*, 225.
(39) Raczkowska, J.; Bernasik, A.; Budkowski, A.; Sajewicz, K.; Penc, B.; Lekki, J.; Lekka, M.; Rysz, J.; Kowalski, K.; Czuba, P. *Macromolecules* **2004**, *37*, 7308.
(40) Jukes, P. C.; Heriot, S. Y.; Sharp, J. S.; Jones, R. A. L. *Macromolecules* **2005**, *38*, 2030.
(41) Heriot, S. Y.; Jones, R. A. L. *Nat. Mater.* **2005**, *4*, 782.

(42) Raczkowska, J.; Budkowski, A.; Rysz, J.; Czuba, P.; Lekka, M.; Bernasik, A. *J. Nanostr. Polym. Nanocomp.* **2005**, *1*, 23.
(43) Segalman, R. A.; Yokoyama, H.; Kramer, E. J. *Adv. Mater.* **2001**, *13*, 1152.
(44) Cheng, J. Y.; Ross, C. A.; Thomas, E. L.; Smith, H. I.; Vansco, G. J. *Appl. Phys. Lett.* **2002**, *81*, 3657.
(45) Xia, Y.; Whitesides, G. M. *Angew. Chem., Int. Ed.* **1998**, *37*, 550.
(46) Bernasik, A.; Rysz, J.; Budkowski, A.; Kowalski, K.; Camra, J.; Jedliński, J. *Macromol. Rapid Commun.* **2001**, *22*, 829−834.
(47) Wang, P.; Koberstein, J. T. *Macromolecules* **2004**, *37*, 5671.
(48) Vainstein, B. K. *Modern Crystallography I*; Springer-Verlag: New York, 1981.
(49) For 1-dim 'unit cell' with 2 atoms (at $x_1 = 0$, and $x_2 = 1/2$) with identical atomic factor f, the structure amplitude $F_2(h) = f[\exp(i2\pi hx_1) + \exp(i2\pi hx_1)] = f[1 + \exp(i\pi h)] = 0$ for $h = 1$.[48] Simulations, performed by another FFT program (available with ref 50), show this relation to hold (within typical I_n uncertainties of Figure 4) when atomic factors (peak areas in Figure 6e) differ less than ∼45%.
(50) Silsbee, R. H.; Dräger, J. *Simulations for Solid State Physics*; Cambridge University Press: Cambridge, U.K., 1997.
(51) Farber, L.; Levin, I.; Borisevich, A.; Grey, I. E.; Roth, R. S.; Davies, P. K. *J. Solid State Chem.* **2002**, *166*, 81 and references therein.
(52) For 1-dim 'unit cell' with 3 identical atoms (at $x_1 = 0$, $x_2 = 1/3$, and $x_3 = 2/3$) the structure amplitude $F_3(h) = f[1 + \exp(i2\pi h/3) + \exp(i4\pi h/3)] = 0$ for $h = 1$.[48] Hence for intergrowth structure the structure amplitude $F(h) = aF_2(h) + bF_3(h) = 0$ for $h = 1$ ($a + b = 1$).

MA062614F